Atomic scale insight on the increased stability of tungsten modified platinum/carbon fuel cell catalysts

Elena Willinger[a,b], Youngmi Yi[b], Andrey Tarasov[a], Raoul Blume[b], Cyriac Massué[b], Frank Girgsdies[a], Claudia Querner[c], Ekkehard Schwab[c], Robert Schlögl[a,b] and Marc-Georg Willinger*[a,b]

Abstract: The limited stability of carbon supported Pt catalysts for oxygen reduction reaction (ORR) is a key obstacle for their commercial application in fuel cells. Here we report on the properties of a tungsten modified Pt/C catalyst that shows enhanced stability under potential cycling conditions compared to a reference Pt/C catalyst. While routine structural investigation by XRD and TEM show an inhomogeneous distribution of tungsten species on the modified catalyst surface, XPS points to an overall changed catalytic behavior of Pt nanoparticles. Aberration corrected atomic scale imaging reveals the presence of homogeneously dispersed tungsten atomic species that decorate the surface of the carbon support and the Pt nanoparticles. The presented results demonstrate that detailed and localized imaging at the atomic scale is essential for the identification of relevant species amongst spectator phases and thus, for the understanding of reasons for an improved integral behavior of a modified catalyst.

Introduction

Pt nanoparticles dispersed on a conductive, high surface area carbon support (Pt/C) are state of the art electrode catalysts for the oxygen reduction reaction (ORR) taking place at the cathode side of low temperature proton exchange membrane fuel cells (PEMFC)[1]. However, a major obstacle for the industrial application of present Pt/C based PEMFC lies in their insufficient durability under realistic operation conditions and the high cost of platinum. The performance degradation is a consequence of the rapid and significant loss of the platinum electrochemically active surface area (ECSA) due to corrosion of the carbon support as well as Pt detachment through electrochemical dissolution, Ostwald ripening, and aggregation[2] over time.

Several strategies have been followed in order to improve the durability of cathode catalysts. Amongst them, the alloying or modification of Pt with other transition metals,[3, 4] as well as the development of new durable catalyst supports,[5, 6] and utilization of Pt-based catalysts with new morphologies[7] have shown their potential. Recently, Zhang et al. employed an electrochemical underpotential deposition method to decorate carbon-supported Pt nanoparticles with small amounts of metallic Au clusters.[8] They found that the modification of Pt nanoparticles by Au clusters prevents Pt oxidation and significantly improves the catalyst durability during the ORR. Similar results were reported by Ye Zhang et al., where the modification of carbon-supported Pt nanoparticles by small amounts of Au species significantly improved not only thermal stability but also electrochemical durability for the ORR.[9] Furthermore, the decoration of bimetallic carbon supported catalysts with Pt[10] and Ir[11] metals was shown to result in enhanced stability and activity in ORR.

These examples from the literature underline that the structural and compositional modification of Pt/C catalysts with other transition metals can lead to significantly improved catalytic characteristics. These effects arise because the presence of other metals around a parent metal changes its electronic environment, resulting in modification of its electronic structure and consequently, its chemical properties.[12] For ORR, a slight downshift of the d-band center for Pt supported on 3d-metal alloys was shown to result in a weaker oxygen adsorption on the surface.[13] Indeed, the strength of oxygen adsorption is a very important parameter, because if oxygen binds too strongly to the cathode, it could poison the surface and reduce its catalytic activity. Tada et al. have investigated elementary steps of the ORR on a Pt/C and Pt_3Co/C cathode catalyst.[14, 15] In their study, it has been shown that the addition of Co to Pt leads to a large increase in the rate constants for the reduction process of Pt−O bond breaking, and Pt−Pt bond reformation. Kitchin and Nørskov have reported that the adsorption energy of many small molecules for bimetallic systems decreases as the surface d-band center lowers in energy.[12, 16] Therefore, the combination of Pt with other transition metals can be used to tune its catalytic properties through a modification of its surface d-band structure.

Tungsten carbide is one of the promising candidates for developing new Pt-based composite electrode catalysts. In the past 40 years it has been discovered that low cost tungsten carbide exhibits properties in several catalytic reactions that are similar to Pt.[17] In addition, it has been reported by Liang et al. that synergistic effects between Pt, WC_x and CNTs induce a higher electrocatalytic activity for the ORR and a better immunity to methanol compared to Pt/CNT catalysts.[18] Furthermore, it was demonstrated that W_2C can serve as electronic promoter that prevents Pt from oxidation and modifies the Pt d-band structure via charge flow from W_2C to Pt.[19]

First principle DFT calculations confirm that a strong metal-support interaction of Pt single-atoms deposited on low-indexed W_xC surface leads to the downshift of the d-band center and to thermodynamically favorable oxygen dissociation.[20] Regardless of the many descriptions about the consequences and reasons of W modification, actual confirmation by direct visualization of the relevant species on the atomic scale is still missing.

[a] Dr. E. Willinger, Dr. Y.Yi, Dr. A. Tarasov, Cyriac Massué, Dr. Frank Girgsdies and Prof. Dr. R. Schlögl,
Dr. M.-G. Willinger
Department of Inorganic Chemistry
Fritz Haber Institute of the Max Planck Society
Faradayweg 4-6, 14195 Berlin (Germany)
Fax:(+49)30- 8413- 4405
E-mail:willinger@fhi-berlin.mpg.de

[b] Dr. E. Willinger, Dr. Y.Yi, Dr. R. Blume, Cyriac Massué, and Prof. Dr. R. Schlögl,
Dr. M.-G. Willinger
Max Planck Institute for Chemical Energy Conversion, Stiftstrasse 34-36, 45470 Mülheim an der Ruhr (Germany)

[c] Dr. Claudia Querner, Dr. Ekkehard Schwab
BASF company, Lüdwigshafen (Germany)

Here we report on the effect of W_xC-modification of a Pt/C catalyst through a detailed study and comparison with a non-modified standard Pt/C as reference. Commercial carbon black was used as substrate for both catalysts. Using analytical transmission electron microscopy techniques (TEM) such as high-resolution (HRTEM) and high-angle annular dark-field (HAADF) imaging in scanning mode (STEM) as well as X-ray diffraction (XRD), X-ray photoelectron spectroscopy (XPS) and temperature programmed oxidation (TPO) we draw conclusions about the reason for the modified electrochemical behavior and improved stability that is revealed by cyclic voltammetry.

Results and Discussion

TEM characterization

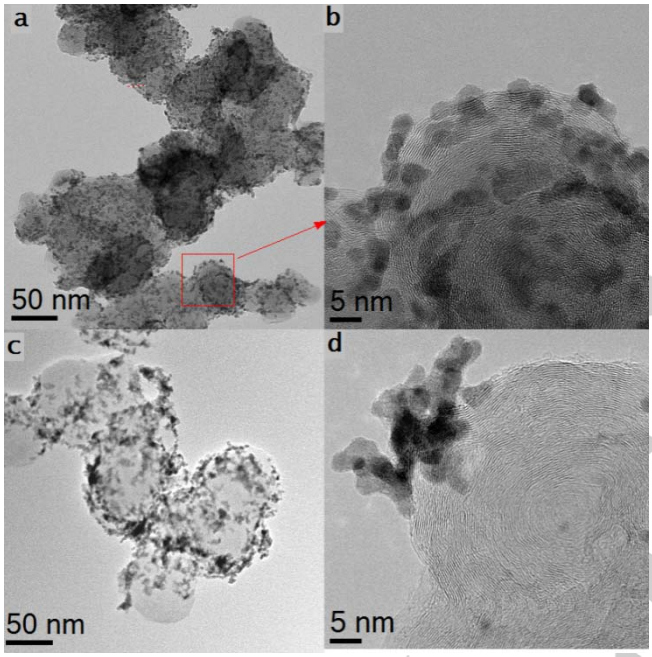

Figure 1. TEM images of PtW_{mod}/C and Pt/C catalysts. a)-b): modified PtW_{mod}/C sample, c)-d): Pt/C reference sample.

Figure 1 shows typical TEM overview images recorded from the modified PtW_{mod}/C (a, b) and the reference Pt/C (c, d) catalysts. The average size of the Pt particles is about 4 nm for both samples. However, their distribution on the carbon support differs for the modified and unmodified sample. Comparative inspection of the TEM images reveals that the standard Pt/C sample shows mainly agglomerated Pt particles, while the modified PtW_{mod}/C contains more homogeneously distributed metal particles. It has to be mentioned here that, due to inherent structural inhomogeneity of the carbon material, a comparison can only be made by considering the dominant structural type of carbon that is present. The investigated carbon black mainly contains agglomerates of spherical particles consisting of concentrically packed defective carbon sheets, such as shown in Fig. 1. From a comparison of similar carbon structures, it is evident that the modified sample shows a better wetting of the carbon support by Pt particles. The HRTEM images of the PtW_{mod}/C (Figure. 1b) and the P/C (Figure. 1d) clearly demonstrate this difference. TEM analysis therefore suggests a stronger metal-support interaction for the modified PtW_{mod}/C catalyst, which is in agreement with earlier predictions from DFT calculations[20].

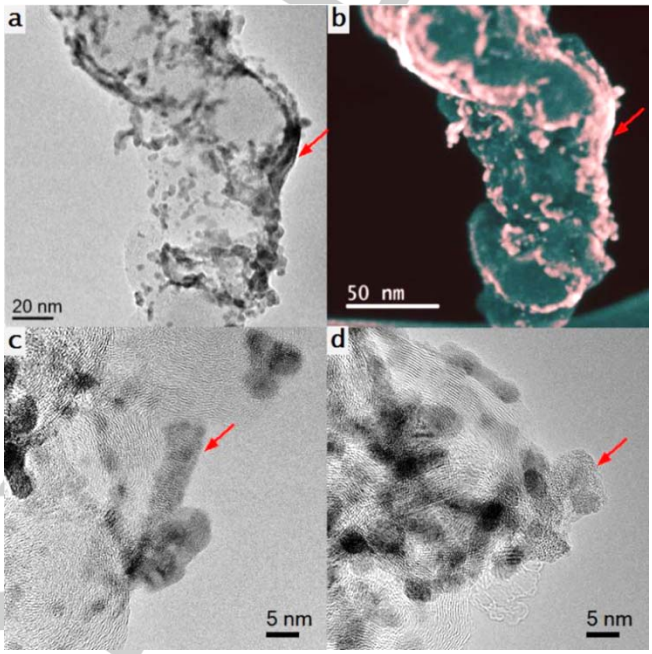

Figure 2. TEM images of PtW_{mod}/C. a) Bright-field STEM and b) SE image showing regions of homogeneous dark contrast due to W-containing deposits (turquoise is carbon support, pink is Pt particles and W-containing deposits). HRTEM images c) and d) reveal the amorphous structure of these W_xC deposits (see arrows).

Figure 2a and 2b show an STEM bright field (BF) and secondary electron (SE) image of the PtW_{mod}/C. Combined they provide information about the carbon structure and its surface topology as well as the distribution of the heavy elements. They thus allow relating the position of the Pt particles to morphological features of the carbon support. Groups of Pt particles often form small aggregates, especially along edge terminated carbon sheets and along borders between soot particles. Varying degree of graphitic ordering and defect density in the carbon structures is responsible for the inhomogeneous distribution of anchoring sites on the surface of the support and hence, for the uneven distribution of platinum particles. Due to tungsten modification, the PtW_{mod}/C sample contains amorphous clusters (marked with an arrow in Figure 2c, d). According to the EDX data, these clusters are partially oxidized and consist of ill-defined W_xCO_y phases (Figure S1). They are irregularly distributed on the surface of the carbon structure, further confirming the structural and chemical inhomogeneity of the carbon support. In some regions, a layer of W_xCO_y covers the C surface, sometimes fully embedding Pt particles (see arrow in Figure 2d).

The XRD pattern of the PtW_{mod}/C and the Pt/C samples (Figure.S2) show that both samples contain broad reflections

due to fcc Pt. The graphite-like phase that appears as a broadened peak (marked CB) is due to the carbon black support. Using the Scherrer equation, a volume weighted average Pt crystallite size of roughly 4nm was estimated for both samples. The value is in good agreement with TEM data. Besides the Pt fcc phase, the XRD pattern of the PtW_{mod}/C modified sample contains sharp reflections due to relatively large crystallites of the WC phase (icsd no.619090).

Overall, quantitative XRD pattern analysis reveals the presence of 11% of the WC phase and 89% of the Pt phase (weight percent). One can see that the obtained mass ratio does not fit to the actual loading with 23.7 wt.% Pt and 32.8 wt.% W (see experimental part). However, considering the TEM data, the modified sample contains a lot of partially oxidized W_xCO_y clusters. These were not considered in the XRD quantification due to their amorphous nature. Taking this fact into account, we have evaluated that nearly 90% of the W is in an amorphous phase. Isolated submicron WC particles were also observed by STEM (see HAADF image in SI, Figure S4). Since they are relatively large and have a low surface area, they are considered as irrelevant spectator phase that does not significantly contribute to the modified behavior of the catalyst.

Electrochemical performance

In order to evaluate the stability of the PtW_{mod}/C modified catalyst under simulated ageing conditions, cyclic voltammetry (CV) experiments were performed. These studies were carried out according to the follow electrochemical corrosion tests[21]: (0.4 – 1.4 V vs. RHE at 1 V/s for 3600 cycles (2 h) and 7200 cycles (4 h) in a 0.1M $HClO_4$. Figure 3 shows electrochemical aging results for the Pt/C, the PtW_{mod}/C and a platinum free W_xC/C reference sample. The W_xC/C reference sample, according to the XRD data, consists of two tungsten carbide phases, namely, 40% of the WC phase and 60% of the W_2C phase (Figure. S3). The recorded CV profiles shown in Figure 3 reveal clear differences between the unmodified and modified samples in the hydrogen desorption region (H_{de}).

Based on electrochemical studies of Pt single crystals, it is known that the hydrogen cathodic peak at about 125 mV is due to so-called “weakly” bonded hydrogen on the Pt (110) surface sites. The peak at 275mV belongs to “strongly” bonded hydrogen and is associated with Pt(100) sites.[22] In general, these regions are used to estimate the electrochemically active surface area. Both peaks are observed in the cyclic profile of the unmodified Pt/C catalyst (Figure 3a), however, the peak at 125 mV is absent in the PtW_{mod}/C sample (Figure 3b). According to the literature, this could be due to tungsten carbide species decorating the (110) of Pt, in a manner similar to the case of bismuth adatoms on Pt particles.[23, 24] The modified PtW_{mod}/C sample furthermore shows a broad anodic peak at about 310 mV, which has been reported to be associated with formation of tungsten bronzes.[25] This peak dramatically decreases after 7200 cycles, indicating surface area loss of oxidized tungsten clusters.

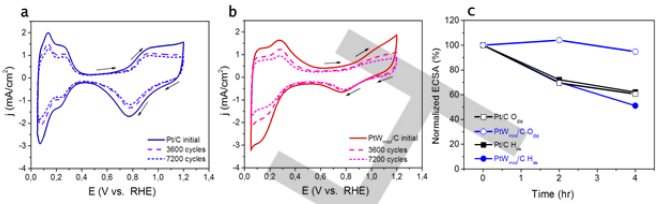

Figure 3. Electrochemical studies on the W modification effect. a-b): CV profiles of the Pt/C and the PtW_{mod}/C catalysts recorded in N_2-saturated 0.1M $HClO_4$ aqueous solution at 50 mV s^{-1}. c): Comparison of the normalized ECSA loss. The filled symbols are determined using the H_{de} area, while open symbols are determined by the O_2 desorption area abstracted in the corresponding cycling voltammetry profiles.

Shao et al demonstrated the dissolution of about 40% of the total W loading under similar potential cycling conditions for their Pt/WC/C catalyst.[26] A similar mechanism of electrochemical surface area loss is thus assumed for the W_xCO_y amorphous clusters on the PtW_{mod}/C sample. Moreover, due to overlapping contributions from Pt and W, the sweep region associated with (H_{de}) is not suitable for an estimation of the Pt active surface area in the W modified sample. On the other hand, it is known that WC, W_2C and WO_3 do not show catalytic activity in the oxygen reduction reaction. [27-29] This is confirmed by the electrochemical curve of the Pt-free W_xC/C sample in that potential region (Figure S5). Thus, this region of oxygen desorption on the cathodic sweep at 0.8 V can be used as an alternative for the estimation of the Pt electrochemical active surface area (ECSA).

Figure 3c shows the ECSA abstracted for Pt/C (black lines) and PtW_{mod}/C (blue lines) samples. The filled symbols correspond to the ECSA estimation based on the H_{de} area, while the open symbols correspond to the ESCA abstracted from the O_{de} area. The details of ECSA calculations are shown in the supporting information (Figure S6). Perfect coincidence of the ECSA values estimated via the two methods for the Pt/C sample indicates that the use of the oxygen desorption area is indeed justified. From the comparison of the ECSA loss based on the O_{de} area for the PtW_{mod}/C and Pt/C, one can see that there is just about 5% of Pt ECSA loss in the PtW_{mod}/C, compared to an almost 40% ECSA loss in the Pt/C samples. HAADF images recorded after electrochemical ageing (Figure S7a) confirm the significant loss of Pt particles in the case of the Pt/C catalyst. In contrast, nearly no change in particle loading and distribution was observed for the PtW_{mod}/C sample (Figure S7b). Thus, the surface modification with tungsten significantly increases the stability with respect to the conventional Pt/C catalyst, preventing detachment of Pt particles from the carbon support.

Temperature programmed oxidation

Thermoanalytical measurements were performed in order to assess the thermal stability of conventional Pt/C and modified PtW_{mod}/C against oxidation. Heating was performed in a 21% O_2 in Ar gas flow at atmospheric pressure and a heating rate of 5 °C/min from room temperature up to 1000 °C. For comparison, TPO analysis has also been performed for pure carbon black

and Pt-free W_xC/C modified carbon black. The profiles of weight % vs. temperature and the corresponding DSC results are shown in figure 4.

The onset temperature for the carbon combustion reaction differs for the modified and unmodified samples. In the case of platinum free, W_xC modified, and pure carbon black, the onset of the main carbon combustion reaction takes place at 634.8 °C and 685.7 °C, respectively (Figure 4 a). This demonstrates that the added tungsten acts as a catalyst for carbon oxidation, lowering the onset of oxidation by nearly 51 °C. The corresponding DCS profile of the W_xC/C sample shows two additional exothermic peaks at 450 °C and 540 °C.

They are accompanied by a weight gain of nearly 10% and are related to the oxidation process of both, W_xC crystallites and amorphous clusters, up to complete oxidation to WO_3. This was confirmed by XRD analysis of the remaining material after the TPO experiment (Figure S8). The pure Pt/C sample shows the earliest onset for oxidation at 386 °C, reflecting the high activity of Pt (fig.4, blue profiles).

Combination of Pt and W leads to slightly reduced catalytic activity compared to the Pt/C, and the oxidation onset is shifted to 434.7 °C (magenta profiles, Figure 4b). On the DSC curves, an additional shoulder that appears close to the main combustion peak at 460 °C is observed. It coincides with the position of the first exothermic peak of the W_xC/C sample and indicates that some portion of the carbon substrate is in contact with oxidized tungsten species, but out of the influence of platinum. This is in concordance with the TEM investigations that have revealed the presence of inhomogeneously distributed amorphous tungsten-containing clusters, of which some are located apart from platinum particles. Interestingly, no feature due to purely Pt catalyzed C combustion, resulting as a peak at 400 °C in the Pt/C sample, is observed. This indicates that, even though the W_xC appears to be quite inhomogeneously distributed on the surface of the catalyst, the collective of the Pt particles is modified in their activity by the W_xC modification. Indeed, the corresponding thermogravimetric profile shows a different behavior in the weight loss above 450^0C. It is related to the weight gain of the W_xC/C sample in that temperature interval (Figure. 4b) and reflects that the kinetics of the carbon combustion reaction is different in the case of a combined action of platinum and tungsten oxide. The observed increase of the onset for carbon combustion in the case of the W modified Pt/C by nearly 50 °C, compared to the unmodified Pt/C, might be

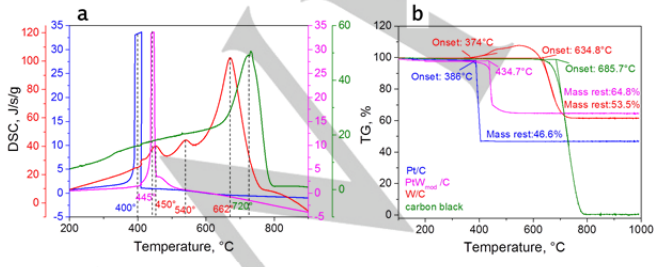

Figure 4. DSC and TG curves of Pt/C, PtW_{mod}/C and W_xC/C and carbon black samples. a) DSC profiles. b) TG profiles

related to the improved electrochemical stability. Irrespective of the inhomogeneous distribution of the amorphous W_xCO_y clusters, there must be an integral effect due to the tungsten modification that has been overlooked by conventional TEM observation.

Atomic scale insight on the tungsten modified Pt/C catalyst

In order to obtain an atomistic view on relevant microstructural details, TEM investigation using Cs corrected instruments was conducted.

Indeed, high resolution TEM, bright-field (BF) and HAADF STEM microscopy examinations revealed the presence of atomic species that are dispersed on the surface of the catalyst. They are irregularly distributed over the carbon surface and also found on the surface of Pt particles (Figure 5 a-c). HRTEM imaging clearly shows that the surface of Pt particles and the Pt-C interface exhibits atoms with specific strong contrast, such as indicated by red arrows in Figure 5a and b. These atomic species can nicely be seen in the corresponding HAADF image (Figure 5c). The nature of this atomic species was identified by EDX mapping. As shown in figure 5, the surface decoration is due to tungsten and thus, a consequence of the modification. As mentioned above, the modified sample exhibits a better Pt-carbon interaction, which is manifested by a better wetting. On the basis of the atomically resolved images we therefore assume that the tungsten species forms a hetero-interface between platinum and carbon, resulting in an increased metal-support interaction. It is known that a change of the metal-support interaction involves modification of the electronic structure and can thus induce changes in the adsorptive properties of a system. [30] It is therefore likely that these clusters are the reason for the integrally different behaviour of the PtW_{mod}/C catalyst. In order to collect further evidence, XPS measurements were performed.

X-ray photoelectron spectroscopy

Figure 6 (a, b) shows a comparison of Pt4f XPS spectra recorded at room temperature and at 110 °C for the Pt/C and the modified PtW_{mod}/C samples, respectively. From the deconvolution of intensity profiles recorded at room temperature, it follows that the surface of the Pt/C catalyst contains PtO_2/PtO and/or PtOH states, while the PtW_{mod}/C modified sample mainly shows the presence of metallic Pt. This finding is in agreement with the literature, according to which W has the tendency to preserve the metallic state of Pt.[31-33] *In-situ* heating of the samples to 110 °C inside the XPS chamber leads to desorption of surface species and reduction of Pt from PtO_2/PtO and/or PtOH states. After low temperature annealing, both samples show platinum in metallic state. The W 4f XPS measurements are shown in Figure 6c. The peak profiles can be decomposed into two pairs of peaks, corresponding to the typical binding energies of $W^{6+}$and W^{5+}, respectively [34].

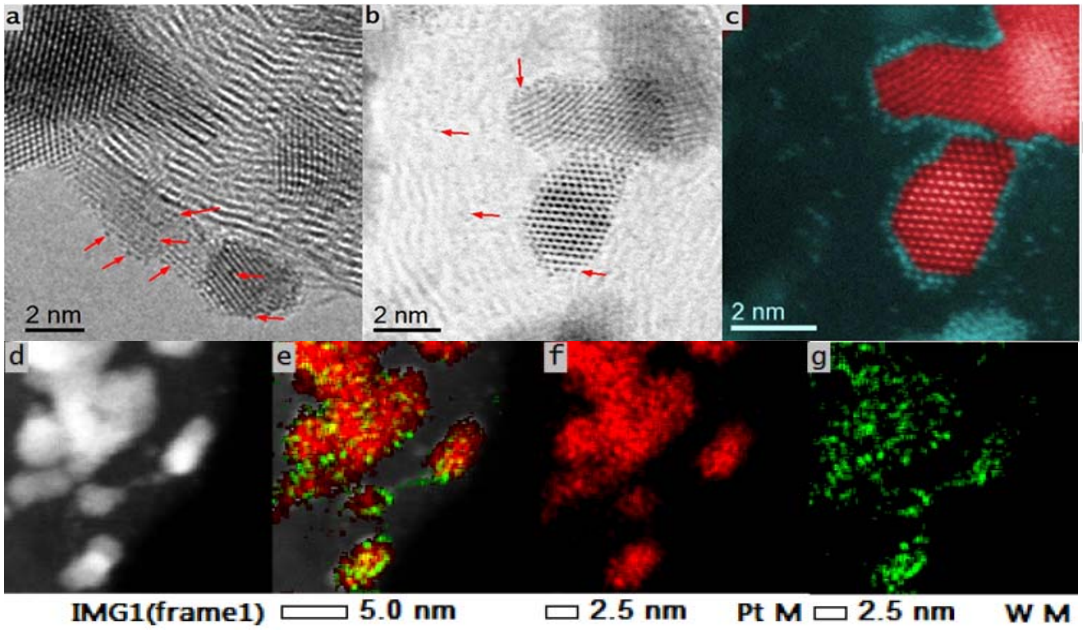

Figure. 5. High-resolution STEM micrographs of PtW_{mod}/C modified sample, showing decoration of Pt particles with atomic species; a) HRTEM, b) BF, c) HAADF (turquoise corresponds to tungsten species, red to Pt particles) image, respectively, d-g) HAADF image and corresponding EDX mapping results of modified PtW_{mod}/C sample showing that observed atomic species belong to tungsten (red is Pt, green is W).

With heating, the part related to W^{5+}states disappeared. Instead, a minor intensity feature, which is attributed to the W^{4+} oxidation state, appeared at the lower binding energy side. No trace of WC, which should be located at ~32eV, was observed. Overall, XPS reveals a tungsten surface state that corresponds to that of WO_3. This finding is in agreement with the HAADF STEM data that shows a core-shell structure of the submicron WC crystals with an oxidized surface layer (Figure S4). Taking into account the majority of W is contained in oxidized WC crystals and partially oxidized amorphous W_xCO_y clusters, the nature of the small fraction of W, which is distributed as atomic species on the surface of the platinum and carbon, cannot be revealed by XPS. However, the chemical state of the Pt surface is clearly affected by the presence of homogeneously dispersed atomic tungsten species. They give rise to an increased resistance of the Pt particles against oxidation. Thus, the XPS results provide a possible explanation for the increased electrochemical and thermal stability of the modified PtW_{mod}/C catalyst.

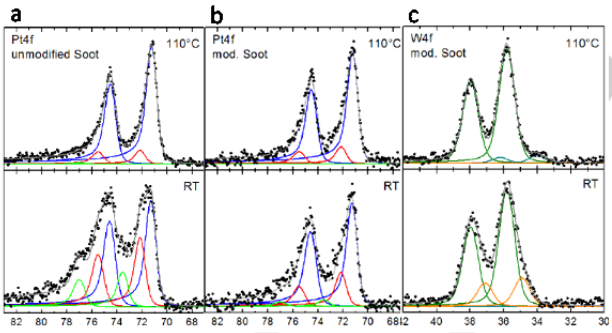

Figure 6. XPS spectra of Pt 4f and W4f measured at room temperature (RT) and after annealing at 110^0 C: a) Pt4f of the pure Pt/C catalyst; b) Pt4f of PtW_{mod}/C modified catalyst. The black experimental curves are deconvoluted into peaks corresponding to Pt^0 metallic states (blue curves), Pt^{2+} states (red curves) due to formation of $PtO/Pt(OH)_2$ and to Pt^{4+} states (green curves) due to PtO_2/OH groups ; c) W4f XPS spectra deconvoluted into W^{6+} states due to WO_3 phase (light green curves), W^{5+} states (orange curve) and W^{4+} due to WO_2 phase (dark green curve).

TEM after electrochemical ageing:

To better understand how electrochemical stability correlates with structural and compositional changes, atomic resolution HAADF STEM and EDX measurements were performed after electrochemical ageing. As already mentioned, the detachment and sintering of Pt particles is reduced in the case of the modified Pt/C (Figure S6). This observation confirms the interpretation of the CV data. After the corrosion tests, the surface of the carbon support still shows the presence of small clusters of strongly scattering atom size clusters. Some of them are in close proximity to Pt particles.

EDX mapping and line scans demonstrate that these small crystalline clusters are due to a W-containing phase (see Figure 7 c-d). HAADF STEM images show that both, large amorphous clusters with W as well as smaller W-clusters that are found in the proximity of platinum particles, exhibit structural order after electrochemical ageing (Figure S9). Due to a weak crystallinity, it is difficult to assign a phase to these tungsten clusters, however, under oxidative conditions of electrochemical ageing, the formation of a tungsten oxide is expected. Moreover, some

of the relatively big tungsten particles show a well-ordered crystalline structure of WO_2 phase (Figure S10) after electrochemical ageing. A complete oxidation of tungsten-containing phases was observed during the TPO experiment, where XRD of the final product revealed the presence of metallic Pt and WO_3 (see Figure S8).

The possible function of the W modifier

The collected results provide evidence for a multiple function of the W modifier. They can be summarized as schematically shown in figure 8. The WC crystalline phase (blue boxes in Fig. 8) is clearly identified by XRD. It acts merely as a spectator phase and has no detectable influence on the behavior of the modified catalyst. A large amount of W is confined in the amorphous rafts and extended clusters. Although initially in the form of WC_x, they oxidize with time towards WO_3. This species shows dominant contributions to the current density in the hydrogen desorption regime, but has no modifying effect on the catalytic properties of the Pt. However, it might act as a reservoir for atomic W species. Finally, we are left with a twin function of the well-dispersed atomic W species that are decorating the surface of the carbon support. They are attached at defect sites of the carbon structure and are also found at the interface between Pt and carbon. At the interface, they act as a bridge, providing a good anchoring of the Pt particles. Although analytically not accessible, they could be in the form of a carbide, with the advantage of being a good conductor. They are likely the reason for an improved distribution and wetting of Pt in the case of the modified sample.

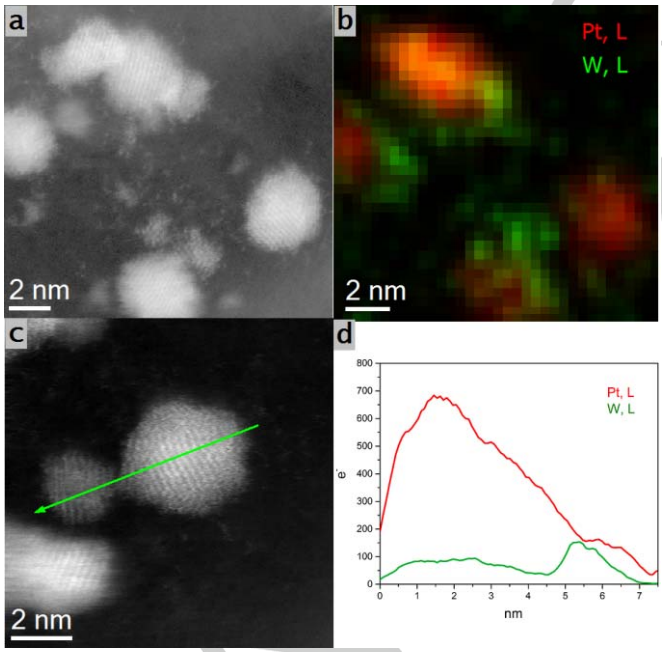

Figure 7. HAADF STEM images and corresponding EDX map and line scan profiles of the PtW_{mod}/C sample after CV measurement: a), c) HAADF STEM images; b) EDX map; d) EDX line scan.

The second function of the atomic W species is related to partially oxidized WO_x species. They can act at the outer Pt-gas interface to form there an oxide termination layer of about one W atom thickness. This is a functional species that acts as geometric modifier of high index Pt facets and may prevent the formation of Pt hydroxides, and finally, oxides that destroy the stability of the nanoparticles. These species may be directly involved in the electro-catalysis by acting as fixation for OH groups and supporting their dissociation: W oxides in contact with water are Broensted acids and help breaking O-H bonds certainly better than Pt metal.
Finally, such a termination layer creates wetting contact between Pt and the water electrolyte and may thus prevent specific adsorption of counter ions from the electrolyte.

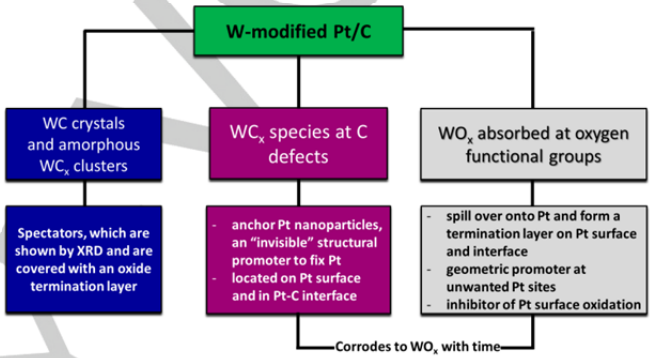

Figure.8 The Scheme of possible functions of the W modifier.

Conclusions

The combination of XPS and high-resolution analytical electron microscopy techniques has shown that the altered performance of a modified PtW_{mod}/C catalyst compared to a standard Pt/C catalyst is a consequence of the decoration of Pt particles with atomic tungsten species. The W species have the two main functions of providing a better anchoring of Pt nanoparticles to the carbon support and to prevent oxidation of Pt by promoting O-H bond breaking and slightly altering the catalytic activity of the Pt particles. The findings are therefore in agreement with experimental results and theoretical predictions in the literature. However, here we were able, by combining atomic scale investigation and complementary analytical techniques, to identify and localize the relevant modifier and to distinguish it from spectator phases. The identification of a relevant species is important for the optimization of catalyst synthesis and for the understanding of the function of individual constituents and synergistic effects between them.

Experimental Section

The local chemical composition and microstructure of the samples before and after electrochemical corrosion tests were investigated by analytical electron microscopy using a FEI Titan 80-300 equipped with an image C_s corrector and with a double Cs-corrected JEOL JEM-ARM200CF scanning transmission electron microscope with a cold FEG. The instruments were operated at, respectively, 300 kV and 200 kV. Energy dispersive X-ray spectra were recorded with a Silicon Drift EDX detector.

For electron microscopy, the samples were dispersed in chloroform and drop deposited onto holey carbon coated copper support grids. The EDX line scans were recorded at a step size of 3 Å with a dwell time of 1 sec/step. EDX maps were recorded at a step size of about 3 Å and 0.5 sec dwell time.

Simultaneous TG–DSC was carried out on a NETZSCH STA 449C Jupiter thermo-analyzer equipped with an electromagnetic microbalance with top loading. The TG resolution was 0.1 µg. The relative error of mass determination was 0.5%. A highly sensitive disk-shaped sample carrier with Pt/Pt–Rh thermocouples was used. Measurements were taken in the temperature range from 30 to 1000^0 C under a controlled Ar/O_2 flow of 79:21 Nml/min at a heating rate of 5 ^{0}C/min. The purity of the gases used in the experiments were Ar (99.999%) and O_2 (99.999%). Temperature and heat calibration was performed with pure metallic standards (In, Sn, Bi, Zn, Al, Au). Samples of 10–15 mg were positioned into corundum crucibles (85 µl) without lids. The apparatus was equipped with a Pfeiffer QMS200 Omnistar mass spectrometer for gas phase analysis.

The XRD data were measured at room temperature using a Bruker D8 Advance diffractometer with CuK_α radiation. The phase quantitative analysis was performed with PowderCell 2.4 and TOPAS (Bruker AXS) software.

The electrochemical measurements were conducted in a three-compartment electrochemical Teflon-cell, using a rotating disc electrode (RDE) setup. A Pt-wire was used as a counter electrode and a Saturated Calomel Electrode (SCE) as reference electrode. $HClO_4$ 0,1M was used as electrolyte with the option of bubbling constant streams of N_2 through the solution. Working electrodes were prepared by depositing defined volumes of catalyst ink on a glassy carbon RDE (electrode diameter is 6 mm and the electrode area is 0.2826 cm^2) and drying them at 60°C for 30 min. The targeted loading is 20 µg(Pt)/cm^2. Catalyst inks were prepared by sonication for 30 min a suspension of 8mg of catalyst powder in 2 mL of water, 2.98 mL of iPrOH and 20 µL of a Nafion 5% solution. Prepared electrodes were pretreated in the EC-cell in N_2-saturated electrolyte by cycling the working electrode potential from 0.05 to 1.2V vs. reversible hydrogen electrode (RHE) 50 times at 100mV/s. CV measurements were recorded afterwards at 50mV/s between 0.05 and 1.4V vs. RHE. The stability test was performed between 0.4 and 1.4V vs reversible hydrogen electrode (RHE) with a scan rate: 50 mV/s for 3600 and 7200 cycles to evaluate the ECSA change.

The XPS experiments were performed in the NAP-XPS setup at the ISISS beamline of the FHI located at the BESSY II synchrotron radiation facility in Berlin, Germany. The setup consists of a reaction cell attached to a set of differentially pumped electrostatic lenses and a separately pumped analyzer (Phoibos 150 Plus, SPECS GmbH), as described elsewhere.[35] The spectra were collected in normal emission in vacuum with a probe size of ~ 150 µm × 80 µm. The samples were heated from the back using an external IR-laser (cw mode, 808 nm). The temperature was controlled via a K-type thermocouple in direct contact with the sample surface. Possible sample contamination was checked by survey spectra at the beginning of each experiment. For the Pt4f spectra photon energies of hv = 250 eV was chosen corresponding to a total XPS information depths of ≈ 2 nm. That is, 95% of all detected electrons originate from a depth of 3λ below the sample surface.[36] Background correction was performed by using a Shirley background.[37] The C1s spectra were fitted following the Levenberg-Marquardt algorithm to minimize the χ^2. Peak shapes were modelled by using Doniach-Sùnjić functions convoluted with Gaussian profiles so that an asymmetric line shape could be fitted when required.[38] The accuracy of the fitted peak positions is ≈ 0.05-0.1 eV.

Surface modification of carbon black by tungsten carbide was done from ammonium heptatungstate using urea. 14 g of ammonium heptatungstate and 15.3 g of urea were dissolved in 300 ml of water. 10 g of carbon black were subsequently added and the mixture was homogenized using and Ultra-Turrax at 8000 rpm for 15 minutes. The mixture obtained in this way was concentrated on a rotary evaporator until a viscous mass had been obtained, and this mass was then heated in a tube furnace firstly at 100^{o}C for 2 hours under a nitrogen atmosphere and subsequently annealed at 850^{o}C for 6 hours (patent No: US 8709964B2). All investigated catalysts were synthesized by BASF SE, Germany. As the yield of the reaction was not known, the actual loading was determined on the basis of the mass rest after thermogravimetric oxidation and its quantitative XRD analysis. The actual Pt loading in the reference Pt/C catalyst was 46.6 wt%. The modified PtW_{mod}/C catalyst contained 23.7 wt% of Pt and 32.8 wt% of W. The platinum-free reference W_xC/C catalyst consisted of 42.4 +-2 wt% W.

Keywords: oxygen reduction reaction, Pt/C modification, tungsten carbide, catalyst durability, HRTEM, EDX

[1] X. W. Yu and S. Y. Ye, *Journal of Power Sources* **2007**, *172*, 133-144.

[2] J. C. Meier, C. Galeano, I. Katsounaros, A. A. Topalov, A. Kostka, F. Schuth and K. J. J. Mayrhofer, *Acs Catalysis* **2012**, *2*, 832-843.

[3] J. X. Wang, H. Inada, L. J. Wu, Y. M. Zhu, Y. M. Choi, P. Liu, W. P. Zhou and R. R. Adzic, *Journal of the American Chemical Society* **2009**, *131*, 17298-17302.

[4] Y. Luo, A. Habrioux, L. Calvillo, G. Granozzi and N. Alonso-Vante, *Chemphyschem* **2014**, *15*, 2136-2144.

[5] H. N. Nong, H. S. Oh, T. Reier, E. Willinger, M. G. Willinger, V. Petkov, D. Teschner and P. Strasser, *Angewandte Chemie-International Edition* **2015**, *54*, 2975-2979.

[6] Z. Sheng, S. Yuyan, L. Xiaohong, N. Zimin, W. Yong, L. Jun, Y. Geping and L. Yuehe, *Journal of Power Sources* **2010**, *195*, 457-460.

[7] C. H. Cui, L. Gan, M. Heggen, S. Rudi and P. Strasser, *Nature Materials* **2013**, *12*, 765-771.

[8] J. Zhang, K. Sasaki, E. Sutter and R. R. Adzic, *Science* **2007**, *315*, 220-222.

[9] Y. Zhang, Q. H. Huang, Z. Q. Zou, J. F. Yang, W. Vogel and H. Yang, *Journal of Physical Chemistry C* **2010**, *114*, 6860-6868.

[10] D. L. Wang, H. L. Xin, Y. C. Yu, H. S. Wang, E. Rus, D. A. Muller and H. D. Abruna, *Journal of the American Chemical Society* **2010**, *132*, 17664-17666.

[11] C. H. Wang, H. C. Hsu and K. C. Wang, *Journal of Colloid and Interface Science* **2014**, *427*, 91-97.

[12] J. R. Kitchin, J. K. Norskov, M. A. Barteau and J. G. Chen, *Journal of Chemical Physics* **2004**, *120*, 10240-10246.

[13] V. Stamenkovic, B. S. Mun, K. J. J. Mayrhofer, P. N. Ross, N. M. Markovic, J. Rossmeisl, J. Greeley and J. K. Norskov, *Angewandte Chemie-International Edition* **2006**, *45*, 2897-2901.

[14] M. Tada, S. Murata, T. Asakoka, K. Hiroshima, K. Okumura, H. Tanida, T. Uruga, H. Nakanishi, S. Matsumoto, Y. Inada, M. Nomura and Y. Iwasawa, *Angewandte Chemie-International Edition* **2007**, *46*, 4310-4315.

[15] N. Ishiguro, T. Saida, T. Uruga, S. Nagamatsu, O. Sekizawa, K. Nitta, T. Yamamoto, S. Ohkoshi, Y. Iwasawa, T. Yokoyama and M. Tada, *Acs Catalysis* **2012**, *2*, 1319-1330.

[16] J. K. Norskov, T. Bligaard, A. Logadottir, S. Bahn, L. B. Hansen, M. Bollinger, H. Bengaard, B. Hammer, Z. Sljivancanin, M. Mavrikakis, Y. Xu, S. Dahl and C. J. H. Jacobsen, *Journal of Catalysis* **2002**, *209*, 275-278.
[17] R. B. Levy and M. Boudart, *Science* **1973**, *181*, 547-549.
[18] C. H. Liang, L. Ding, C. A. Li, M. Pang, D. S. Su, W. Z. Li and Y. M. Wang, *Energy & Environmental Science* **2010**, *3*, 1121-1127.
[19] C. K. Poh, S. H. Lim, Z. Q. Tian, L. F. Lai, Y. P. Feng, Z. X. Shen and J. Y. Lin, *Nano Energy* **2013**, *2*, 28-39.
[20] C. K. Poh, S. H. Lim, J. Y. Lin and Y. P. Feng, *Journal of Physical Chemistry C* **2014**, *118*, 13525-13538.
[21] K. Hartl, M. Hanzlik and M. Arenz, *Energy & Environmental Science* **2011**, *4*, 234-238.
[22] J. Clavilier, D. Armand, S. G. Sun and M. Petit, *Journal of Electroanalytical Chemistry* **1986**, *205*, 267-277.
[23] Q. S. Chen, Z. Y. Zhou, F. J. Vidal-Iglesias, J. Solla-Gullon, J. M. Feliu and S. G. Sun, *Journal of the American Chemical Society* **2011**, *133*, 12930-12933.
[24] B. E. Hayden, A. J. Murray, R. Parsons and D. J. Pegg, *Journal of Electroanalytical Chemistry* **1996**, *409*, 51-63.
[25] H. Chhina, S. Campbell and O. Kesler, *Journal of Power Sources* **2007**, *164*, 431-440.
[26] M. H. Shao, B. Merzougui, K. Shoemaker, L. Stolar, L. Protsailo, Z. J. Mellinger, I. J. Hsu and J. G. G. Chen, *Journal of Power Sources* **2011**, *196*, 7426-7434.
[27] Z. Zhonghua, W. Xiaogang, C. Zhiming, L. Changpeng, L. Tianhong and X. Wei, *Journal of Power Sources* **2008**, *185*, 941-945.
[28] M. Hui and S. Pei Kang, *Journal of Physical Chemistry B* **2005**, *109*, 22705-22709.
[29] P. J. Kulesza, B. Grzybowska, M. A. Malik and M. T. Galkowski, *Journal of the Electrochemical Society* **1997**, *144*, 1911-1917.
[30] M. G. Willinger, W. Zhang, O. Bondarchuk, S. Shaikhutdinov, H. J. Freund and R. Schlogl, *Angewandte Chemie-International Edition* **2014**, *53*, 5998-6001.
[31] A. Lewera, L. Timperman, A. Roguska and N. Alonso-Vante, *Journal of Physical Chemistry C* **2011**, *115*, 20153-20159.
[32] F. Wu, Y. H. Liu and C. Wu, *Rare Metals* **2010**, *29*, 255-260.
[33] F. Maillard, E. Peyrelade, Y. Soldo-Olivier, M. Chatenet, E. Chainet and R. Faure, *Electrochimica Acta* **2007**, *52*, 1958-1967.
[34] J. Li, Y. Liu, Z. J. Zhu, G. Z. Zhang, T. Zou, Z. J. Zou, S. P. Zhang, D. W. Zeng and C. S. Xie, *Scientific Reports* **2013**, *3*.
[35] A. Knop-Gericke, E. Kleimenov, M. Havecker, R. Blume, D. Teschner, S. Zafeiratos, R. Schlogl, V. I. Bukhtiyarov, V. V. Kaichev, I. P. Prosvirin, A. I. Nizovskii, H. Bluhm, A. Barinov, P. Dudin and M. Kiskinova in *X-Ray Photoelectron Spectroscopy for Investigation of Heterogeneous Catalytic Processes*, *Vol. 52* Eds.: B. C. Gates and H. Knozinger), Elsevier Academic Press Inc, San Diego, **2009**, pp. 213-272.
[36] M. P. Seah, *Surface and Interface Analysis* **1986**, *9*, 85-98.
[37] D. A. Shirley, *Physical Review B* **1972**, *5*, 4709-&.
[38] S. Doniach and M. Sunjic, *Journal of Physics Part C Solid State Physics* **1970**, *3*, 285-&.

...

Entry for the Table of Contents (Please choose one layout)

Layout 1:

FULL PAPER

In catalysis, the actual effect of promoters is often not very well understood because it is difficult to differentiate between the relevant modifying species and “spectator” phases. Here, we study the effect of tungsten promotion on an industrial Pt/C catalyst. Aberration corrected atomic scale imaging reveals the presence of homogeneously dispersed tungsten atomic species that decorate the surface of the carbon support and Pt nanoparticles.

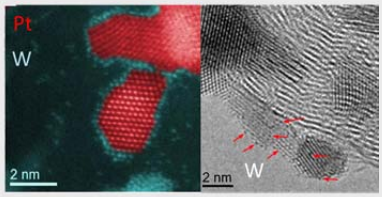

*Elena Willinger, Youngmi Yi, Andrey Tarasov, Raoul Blume, Cyriac Massué, Frank Girgsdies, Claudia Querner, Ekkehard Schwab, Robert Schlög and Marc-Georg Willinger**

Page No. – Page No.

Atomic scale insight on the increased stability of tungsten modified platinum/carbon fuel cell catalysts

Layout 2:

FULL PAPER

*Author(s), Corresponding Author(s)**

Page No. – Page No.

Title